1   *Article*

2 # Surface Plasmon Resonance (SPR) Computational

3 # Study of Hemoglobin (Hb) in Human Blood

4 # Detection

5 **Wida Yanti [1], Kamsul Abraha [2],*and Agung Bambang S.U. [2]**

6   [1]   Departement of Physics, Faculty of Science and Technology, Sunan Kalijaga Islamic State University, Jl
7   Marsda AdiSucipto No.1, Yogyakarta, Indonesia; widayan76@gmail.com
8   [2]   Departement of Physics, Faculty of Mathematic and Natural Science, Gadjah Mada University, Jl Sekip
9   Utara BLS.21, Yogyakarta, Indonesia; kamsul@ugm.ac.id; agungbambang@ugm.ac.id
10   *****   Correspondence: kamsul@ugm.ac.id; Tel.: +62-812-271-0165

11 **Abstract:** A theoretical analysis of haemoglobin (Hb) concentration detection is presented in this
12 work with the objective of achieving more sensitive detection and monitoring low concentrations.
13 Surface-enhanced SPR spectroscopy on silver nanoparticles was employed for recording Hb
14 concentrations less than 10 g/L. In this paper, Fe_3O_4@Au core-shell, nanocomposite spherical
15 nanoparticle consisting of a spherical Fe_3O_4 core covered by Au shell, was used as an active
16 material for biomolecules detection in the *Surface Plasmon Resonance* (SPR)-based biosensor in the
17 wavelength 632.8 nm. We present the simulation of detection amplification technique through
18 *Attenuated Total Reflection* (ATR) spectrum in the Kretschmann configuration. The system consists
19 of a four-layer material i.e prism/Ag/Fe_3O_4@Au+Hb/air. Dielectric function determination of the
20 core-shell nanoparticle (Fe_3O_4@Au) and the composite (Fe_3O_4@Au+Hb) was done by applying the
21 *Effective Medium Theory* approximation and the calculation of the reflectivity is carried out by
22 varying the size of core-shell (r_0). In this simulation, the refractive index of the BK7 prism is 1.51;
23 the refractive index of Ag thin film is 0.13455+3.98651i with the thickness of 40 nm, and the
24 refractive index of the composite is varied depending on the size of nanoparticle core-shell. Our
25 results show that by varying the radius of the core and the shell thickness, the dip of the reflectivity
26 (ATR) spectrum is shifted to the larger angle of incident light and the addition of core-shell in the
27 conventional SPR-based biosensor leads to enhancement of the SPR biosensor sensitivity, for the
28 core-shell radius 10 nm, the sensitivity increased by 1.35% for F = 0.1, and by 4.89% for F =0.8
29 compared to the sensitivity of the conventional SPR-based biosensor without core-shell addition.

30 **Keywords:** Haemoglobin detection; SPR spectroscopy; Biosensors; Computer simulation;
31 Core-shell Fe_3O_4@Au.

32

---

33 **1. Introduction**

34   Currently, there is increasing interest in the development of magnetic and plasmonic
35 nanoparticles as the active materials for biomolecule detection. The new nanoparticle that combines
36 multiple functions or properties not obtainable in the individual material has attracted
37 considerable attention because of its revolutionary technology for sensitivity enhancement of surface
38 plasmon resonance (SPR)-based biosensor [1]. Optical sensor based on SPR is one of the sensitive
39 methods that detects biomolecules and works on the changes of the material refractive index,

40 having fast response, real-time, biospecific interaction analysis and being the label-free technique [2].
41 SPR is a physical process that occurs when the wave vector of the evanescent wave (EW) matches the
42 wave vector of the surface plasmon (SP) under the total internal reflection condition. This resonance
43 condition is expressed as

$$\frac{\omega_0}{c} n_p \sin\theta_{SPR} = \frac{\omega_0}{c}\left(\frac{\varepsilon_m n_d^2}{\varepsilon_m + n_d^2}\right)^{1/2} \qquad (1)$$

46 The variable on left hand side is the propagation constant of a light beam incident at a

47 resonance angle θ_{SPR} through the light coupling device (prism) of refractive index n_p. While the

48 right-hand is the propagation constant with ε_m as real part of the metal permittivity and n_d as the

49 refractive index of dielectric material or sensing medium. ω_0 and c are the light frequency and

50 the speed of the light in the vacuum respectively. The evanescent wave occurs at the metal-dielectric
51 interface when a *p*-polarized wave passes a prism through a metallic layer into a dielectric media.
52 The wave vector of the evanescent wave is a function of refractive indices of the dielectric,
53 metal and analyte i.e the sensing medium. Therefore, if there is a local change in the refractive index
54 of the sensing medium near the metal surface, it will in turn lead to a change in the propagation
55 constant of SP and in the angle of incidence light in order to satisfy the resonance. For applying SPR
56 biosensor, the Kretschmann geometry [3] of Attenuated Total Reflection (ATR) has been found to be
57 very suitable for the sensing and has become the most widely used geometry in SPR biosensor.
58 Mostly, the metallic layer that is used in SPR biosensor measurement consists of either gold or silver.
59 The first demonstration about SPR-based sensor for bio-sensing was reported in 1983 by Liedberg *et*
60 *al* [4]. Several ways to enhance sensitivity of SPR biosensor for detecting biomolecules have been
61 explored for the detection of DNA hybridization [5], acetylcholinesterase [6], membrane protein [7]
62 and human blood-group [8]. SPR can also be a potential candidate for bio-sensing other biological
63 properties such as haemoglobin concentration.
64 From some of researches it is acquired that the conventional SPR-based biosensor was not
65 capable of sensing the small amount biomolecules such as DNA, virus or bacteria [9] due to the poor
66 attachment of biomolecule on the metal surface and the low concentration of it is difficult to detect
67 directly [10]. It happens since the changes in the refractive index of the medium [11] under a thin
68 metal layer are very small. Therefore, the enhancement of sensitivity for detecting small
69 biomolecules can be developed by several approaches such as by involving nanoparticle core-shell
70 as the active material in the conventional SPR-based biosensor. Comparing with nanoparticle which
71 has a spherical shape, the involvement of core-shell aims to avoid polar resonance [12] and to obtain
72 some plasmonic wavelength by varying the radius of the core and the thickness of the shell. A
73 core-shell was said to be a unique material since it is a combination of magnetic and plasmonic
74 materials which has different optical properties between the core and the shell. Some studies have
75 observed, either experimentally or theoretically, about the optical properties of the core-shell with
76 its involvement in the SPR-based biosensor. It is observed that the optical response or resonance
77 spectrum of the core-shell depends on the size of the core and the thickness of the shell. Hence, the

78   core-shell can be used for tuning the plasmonic wavelength [13], e.g $AgSiO_2$ [12], TiO_2@Au and
79   TiO_2@Ag [14]. The study of the optical response of Fe_3O_4@Au core-shell was performed by varying
80   the radius of Fe_3O_4 and the thickness of Au. There was shift resonance spectrum due to the changes
81   of the size of the core and the shell [15]. The core Fe_3O_4 could make the biomolecule attachment
82   easier by the help of its magnetic property, while the shell Au exhibits nontoxicity and compatible
83   property. Furthermore, the performance of the SPR-based biosensor can be enhanced by using the
84   nanoparticle core-shell Fe_3O_4@Au rather using only Fe_3O_4 or only Au. The presence of Fe_3O_4@Au is
85   also capable of enhancing the immobilization of biomolecules e.g Haemoglobin [16], detecting
86   antibody IgG [17] and detecting the DNA of chum salmon [18].. Whereas, involvement of the
87   Fe_3O_4@Au in the SPR-based biosensor was performed for enhancement detection of thrombin [19],
88   and protein concentration of interleukin IL17 [20]. Detection of the haemoglobin concentration has
89   been explored by SPR-based biosensor for three wavelengths (401.5 nm, 589.3 nm and 706.5 nm)
90   with haemoglobin concentration varying between 0 and 140 g/l [21].

91   Due to the coating of Au shell for the magnetic core that protected it from oxidation and
92   aggregation, the stabilization of the core-shell (Fe_3O_4@Au) was enhanced *obviously*. And the current
93   SPR technology has so many advantages as well, i.e processing high sensitivity and selectivity,
94   non-destructive,   large *tunability* from the visible into the *infrared* (IR) spectrum region, label-free
95   analysis and being capable of real-time monitoring. SPR is a kind of electromagnetic resonance that
96   exists when there is an interface between metal and dielectric. This system has been used for sensing
97   various biomolecules [22],[23]. This method is very sensitive to size, shape and the refractive index
98   of surrounding medium or the medium that kept contact with the thin metal layer. When the
99   biomolecule comes in contact with the metal thin film, it is adsorbed on its surface and hence
100   increasing the refractive index at the interface and resulting in a change of the resonance angle.

101   In this paper, we have been investigating the ATR spectrum of three and four multilayer
102   biosensor based on SPR system with Fe_3O_4@Au core-shell addition and the biology element is
103   hemoglobin in the human blood with the refractive index is 1.338 [24]. The different size of
104   Fe_3O_4@Au+Hb composites leads to a change in the SPR resonance angle.

105   This study was focused on the simulation of the effects of the size of the core radius and shell
106   thickness to the effective permittivity of Fe_3O_4@Au. Also, the effects of the volume fraction and the
107   size of the core-shell on the composite effective permittivity and on the SPR-based biosensor
108   reflectivity were investigated. Then, the enhancement of the sensitivity of SPR configuration was
109   estimated.

110   **2. Materials and Methods**

111   2.1. *Kretschmann configuration with four layers*

112   Here, we apply the analytical and computational approximation to calculate reflectivity in the
113   Attenuated Total Reflection (ATR) method and determine the effective permittivity of the composite
114   (the mixture of Fe_3O_4@Au and Hb embedded in the water). In this study, we used the Kretschmann

115   configuration [3] with four layers. i.e prism/Ag/composite/air shown in Figure 1. The angle θ_i and

116   θ_r are the incident and the reflection angle respectively, k_z is the wave vector component along

117   z-axis, and *d* is the thickness of each layer.
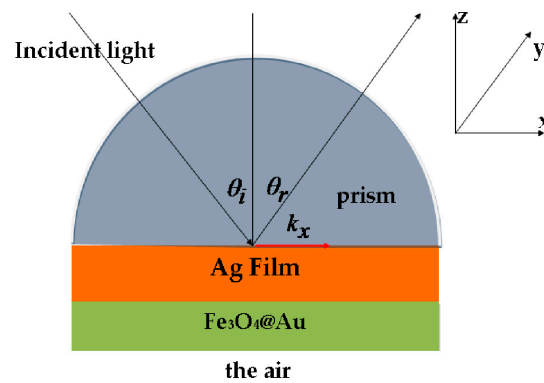
118   **Figure 1.** Kretschmann configuration for SPR-based biosensor with the inclusion of
119   Fe₃O₄@Au core-shell.

120   Figure 2 shows the model of the composite layer containing the inclusion material
121   (Fe₃O₄@Au+biomolecule) and the host material (water). The inclusion material consists of the
122   *scattered grain* material (Fe₃O₄@Au) and the *interfacial shell* material (Hb).
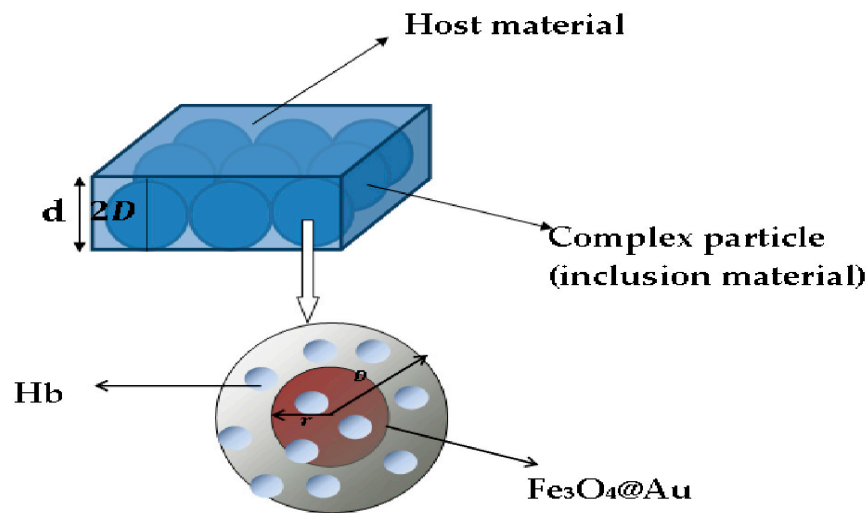
123   **Figure 2.** The composite model contains the complex particle (inclusion)
124   and the host material.

125   In this SPR configuration, the refractive index of the BK7 glass prism is 1.510, the wavelength of
126   the electromagnetic wave is 632.8 nm, the complex refractive index of silver $0.13455+3.98651i$ [25],
127   and dielectric constant of Hb (ε_1) 1.338 for the concentration is less than 10 g/L. The refractive index
128   of water and air is 1.33 and 1.0 respectively [9]. The thickness of Ag film was d=40 nm, and the
129   composite was d=20 nm. The ATR reflectivity R is given by the Fresnel equation [26].

130          $$R = \left| r_{ijk} \right|^2 = \left| \frac{r_{ij}+r_{jk}e^{2ik_{jz}d_j}}{1+r_{ij}r_{jk}e^{2ik_{jz}d_j}} \right|^2 \tag{2}$$

131   with

132
$$r_{ij} = \frac{k_i \varepsilon_j - k_j \varepsilon_i}{k_i \varepsilon_j + k_j \varepsilon_i} \qquad (3)$$

133　here, r_{ij} is the surface reflectivity coefficient between medium i and medium j. k_{ij} is the wave

134　vector component perpendicular to the surface, k_x is the wave vector component parallel to the

135　surface, whereas d_j and ε_i are respectively the j-th layer thickness and the i-th medium dielectric

136　constant.

137　*2.2. The effective permittivity of the spherical Fe₃O₄@Au core-shell*

138　　　Our simulation of the Fe₃O₄@Au core-shell is performed on the model as shown in Figure 3.

139　The magnetic nanoparticle core-shell consists of a Fe₃O₄ core of radius b coated by a metallic Au of

140　thickness $(a - b)$. The dielectric constants of the magnetic nanoparticle and the metallic Au are ε_c,

141　and ε_s , respectively.
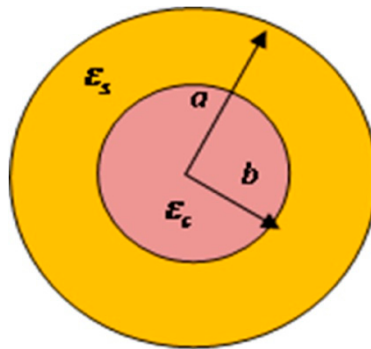
142　**Figure 3.** The model of nanoparticle Fe₃O₄@Au core-shell.

143　whereas, the value of complex ε_c is adopted from Schlegel [27] through reflectivity measurement

144　and Kramers-Kronig relation and ε_s can be quoted from Johnson and Christy work [25]. The

145　effective permittivity $(\varepsilon_{\text{eff}})$ of Fe₃O₄@Au core-shell is derived from the internal homogenization for

146　plasmonic and dielectric constituent material [28], namely

147
$$\varepsilon_{\text{eff}} = \varepsilon_s \frac{a^3 (\varepsilon_c + 2\varepsilon_s) + 2b^3 (\varepsilon_c - \varepsilon_s)}{a^3 (\varepsilon_c + 2\varepsilon_s) - b^3 (\varepsilon_c - \varepsilon_s)} \qquad (4)$$

148　*2.3. Calculating the effective permittivity of the composite*

149　　　The effective permittivity of the composite $(\varepsilon_{\text{eff}})$ is calculated by neglecting the correlation

150　between the inclusion material (complex material or Fe₃O₄@Au+Hb) and host material (water), using

151　the Maxwell Garnett formula [29]

152
$$(1 - F) \frac{\varepsilon_{\text{eff}} - \varepsilon_m}{2\varepsilon_{\text{eff}} + \varepsilon_m} + F \left(\frac{\varepsilon_{\text{eff}} - \varepsilon_n}{\varepsilon_{\text{eff}} + \varepsilon_n} \right) \qquad (5)$$

153　with

154
$$\varepsilon_n = \varepsilon_1 \frac{(2\varepsilon_1 + \varepsilon_2) + 2\alpha(\varepsilon_2 - \varepsilon_1)}{(2\varepsilon_1 + \varepsilon_2) - \alpha(\varepsilon_2 - \varepsilon_1)}$$
(6)

155   where $\alpha = \left(\frac{r_0}{D}\right)^3$, r_0 the radius of Fe_3O_4, D the radius of the complex particle (Fe_3O_4@Au+Hb), F

156   the volume fraction of the inclusion material to the host material, ε_n the dielectric constant of the

157   complex particle and ε_m the dielectric constant of the host material. ε_1 is the Hb dielectric

158   constant as the *interfacial shell*, while ε_2 is the dielectric constant of *scattered grain* (Fe_3O_4@Au

159   *core-shell*).

160   *2.4. Biosensor sensitivity from ATR spectrum*

161   The calculation of the sensitivity of SPR-based biosensor is written as [30]

162

163
$$S = \frac{\Delta\theta_{SPR}}{\Delta n}$$
(7)

164   where $\Delta\theta_{SPR}$ is the difference of the SPR angle and Δn is the change in refractive index.

3. Results and Discussion

166   The changes of the radius of the Fe_3O_4 core and the thickness of the Au shell lead to the change
167   in the effective permittivity of Fe_3O_4@Au core-shell While the change of the inclusion material to
168   host material leads to the change in the effective permittivity of the composite. Therefore, if the
169   complex particle is applied to SPR-based biosensor system, this change leads to the enhancement of
170   the sensitivity of this biosensor. We can show from the reflectivity spectrum that the resonant angle
171   shift to the right.

172   **Table 1**. The effective permittivity of Fe_3O_4@Au *core-shell* for the shell thickness variation.

b (nm)	a (nm)	*Shell thickness* (nm)	$f = (b/a)^3$	ε_{eff} (real , imag)	
10	11	1	0.75	1.0092 , 3.2011	
10	13	3	0.46	-2.5021 , 3.0123	
10	15	5	0.30	-4.8721 , 2.6948	
10	17	7	0.20	-6.4556 , 2.3952	
10	20	10	0.13	-7.9297 , 2.0516	
10	30	20	0.03	-9.7428 , 1.5407	
10	40	30	0.02	-10.212 , 1.3921	
10	100	90	0.001	-10.539 , 1.2845	

173

174   **Table 2**. The effective permittivity of Fe_3O_4@Au *core-shell* for the core radius variation.

b (nm)	a (nm)	$f = (b/a)^3$	ε_{eff} (real , imag)
10	11	0.75	1.0092 , 3.2011
12	13	0.78	1.3637 , 3,2017
14	15	0.81	1.6230 , 3.2000
16	17	0.83	1.8209 , 3.1975
18	19	0.85	1.9768 , 3.1947
20	21	0.86	2.1028 , 3.1921
100	101	0.97	3.0427 , 3.1587

175   **Table 3.** The effective permittivity of Fe_3O_4@Au *core-shell* for the $f = (b/a)^3$ variation.

b (nm)	a (nm)	$f = (b/a)^3$	ε_{eff} (real , imag)
19	20	0.85	2.04008 , 3.19339
18	20	0.73	0.77837 , 3.19889
17	20	0.61	-0.49070 , 3.16118
16	20	0.51	-1.74550 , 3.08115
15	20	0.42	-2.96636 , 2.96227
14	20	0.34	-4.13333 , 2.81043
13	20	0.27	-5.22780 , 2.63368

176   Table 1shows the effective permittivity of core-shell (Eq. 4) for variation in the shell thickness.
177   Table 2 shows the effective permittivity of core-shell for variation in the core radius and Table 3
178   shows the effective permittivity of core-shell for $(b/a)^3$ variation. The data in Tabel 1, , Table 2 and
179   Table 3 are presented in Figure 4, Figure 5 and Figure 6 respectively.
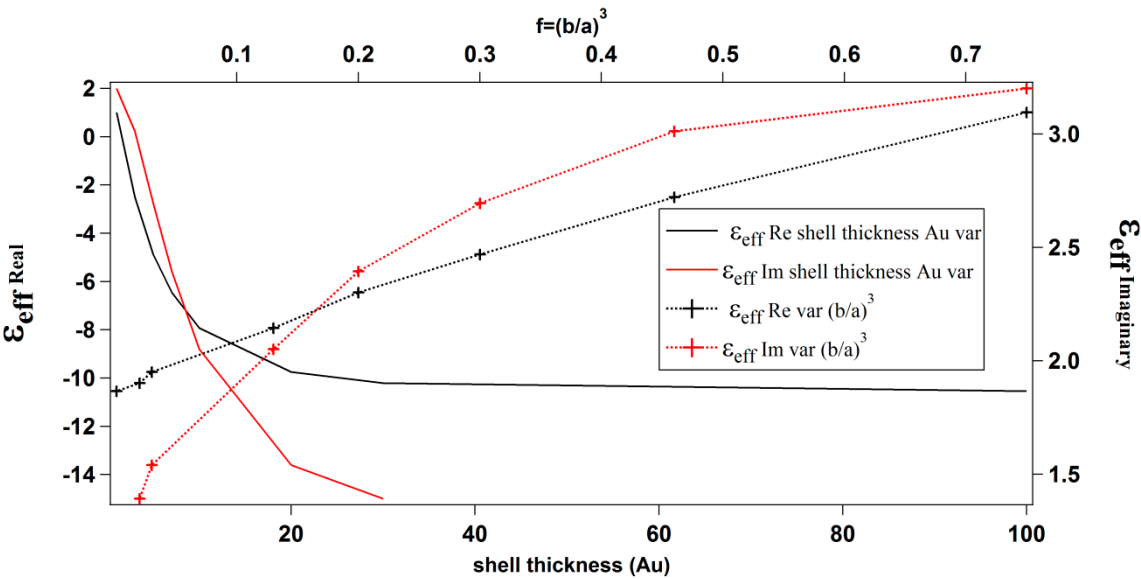
180   **Figure 4**. The effective permittivity of *core-shell* for shell thickness variation and
181          $f = (b/a)^3$ variation.
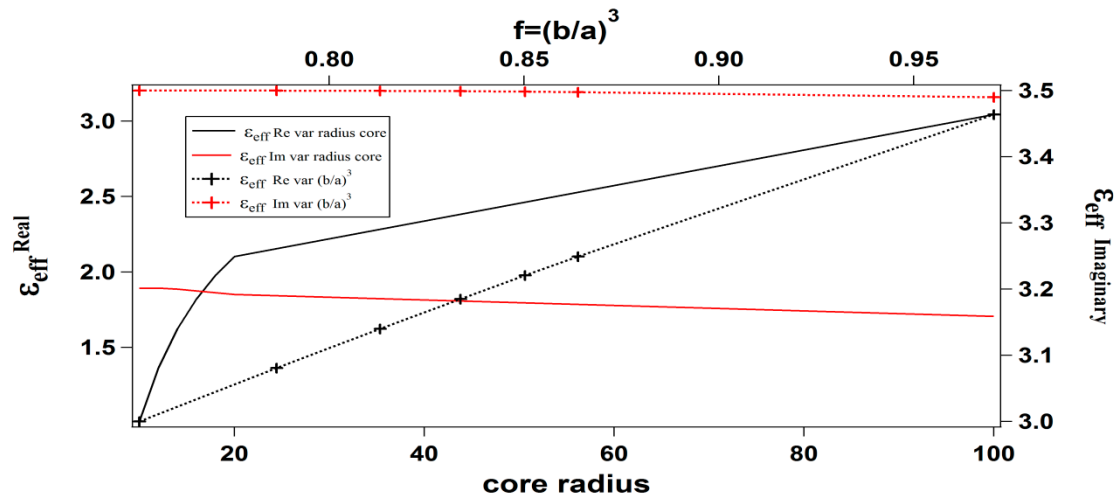
182   **Figure 5**. The effective permittivity of *core-shell* for the radius of the core variation
183   and $f = (b/a)^3$ variation.
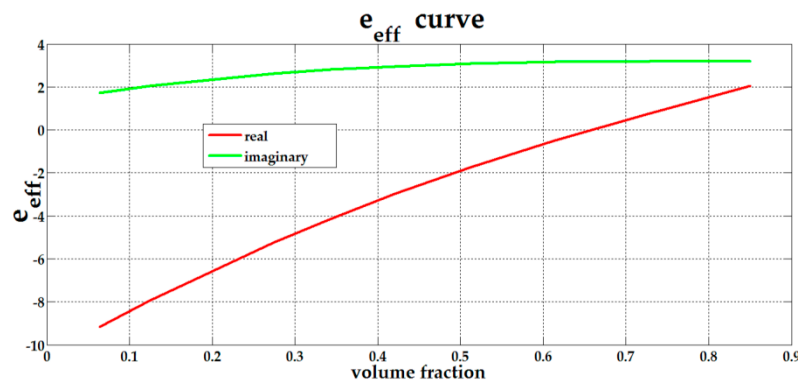
184   **Figure 6**. The effective permittivity of *core-shell* for $f = (b/a)^3$ variation.

185   Figure 4 shows that the increasing shell thickness for fixed core radius (10 nm), leads to the
186   decreasing of the real and imaginary part of the core-shell effective permittivity. But, the real part
187   tends to be constant at the shell thickness above 30 nm. While Figure 5 shows that increasing in the
188   core radius for fixed the shell thickness (1 nm) leads to increasing in the real part of the core-shell
189   effective permittivity while the imaginary part tends to be constant. If the core-shell effective
190   permittivity is viewed only from the $f = (b/a)^3$ variation, it shows that the increasing $f = (b/a)^3$
191   leads to increasing in the real and imaginary parts of the effective permittivity (Figure 6). Different
192   radius of core-shell a (15 nm, 10 nm, 5nm) with the same $f = (b/a)^3$ variation shows the same
193   effective permittivity value. And then the effective permittivity of the composite can be obtained
194   from Eq. 5.
195   The thicknesses of Ag metal in this SPR system is the other parameter that must be carefully
196   controlled in order to obtain an optimum performance for surface plasmon excitation. Therefore the
197   choise of the metal thickness is of greatest importance. By varying the Ag thickness, the ATR
198   spectrum shows where the Ag metal film thickness yields the most desirable resonance peak. As the
199   Ag thickness increases (50 -60 nm), the depth of the resonance peak decrease. This is indicate the
200   reduced coupling efficiency of light into the SP mode on the film. This is due to that the metal begins

201   acting as a reflectance plane when its thickness increases to a point where light cannot couple into
202   the surface charge oscillations that make up the plasmon mode. Whereas, if the Ag thin film is very
203   thin (20-30 nm), it result in more coupling into the SP mode but due to light scattering, the sensitivity
204   was redused. Obviously, from these effects, a compromise must be reached to obtain a satisfactory
205   SPR system. Figure 7 was shows the optimal thickness to support SPR system determined to lie at 40
206   nm.
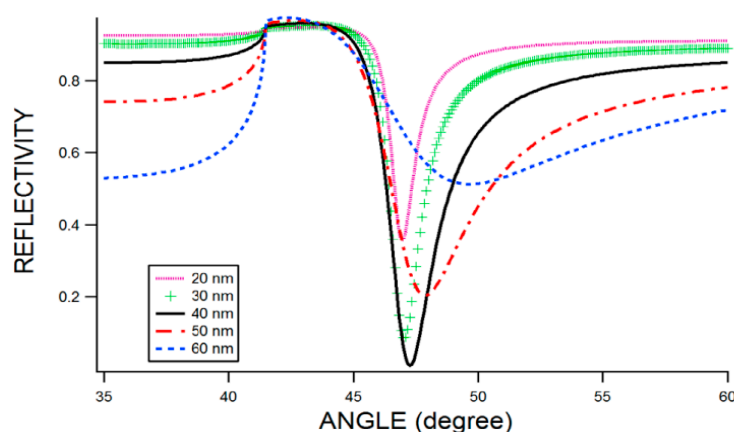
207   **Figure 7**. The ATR spectra for the Ag metal thickness varied from 20 nm to the 60 nm.

208   Based on the above results, we can choose the values of the core radius, the shell thickness and
209   the ratio of the core to the core-shell radius $f = (b/a)^3$ to obtain the desirable effective permittivity
210   of the Fe_3O_4@Au core-shell. Figure 8 and Figure 9 shows the effective permittivity of Fe_3O_4@Au+Hb
211   composite (inclusion material) with volume fraction (F) variation given by the size variation of the
212   core-shell a from 5 nm to 20 nm for fixed $f = (\frac{b}{a})^3 = 0.73$. Here, F is the ratio between the amount of
213   the inclusion material to the host material.

(a)   (b)
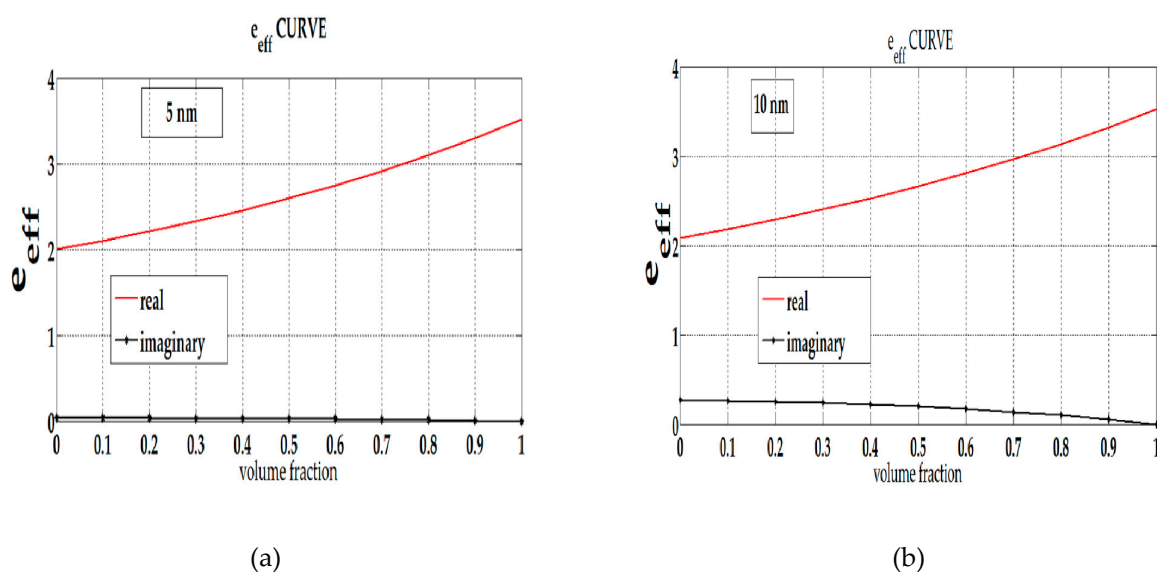
Figure 8. The composite effective permittivity with variation in the volume
fraction (F) of composite for fixed size of the core-shell (a) 5 nm (b) 10 nm.

(a)   (b)
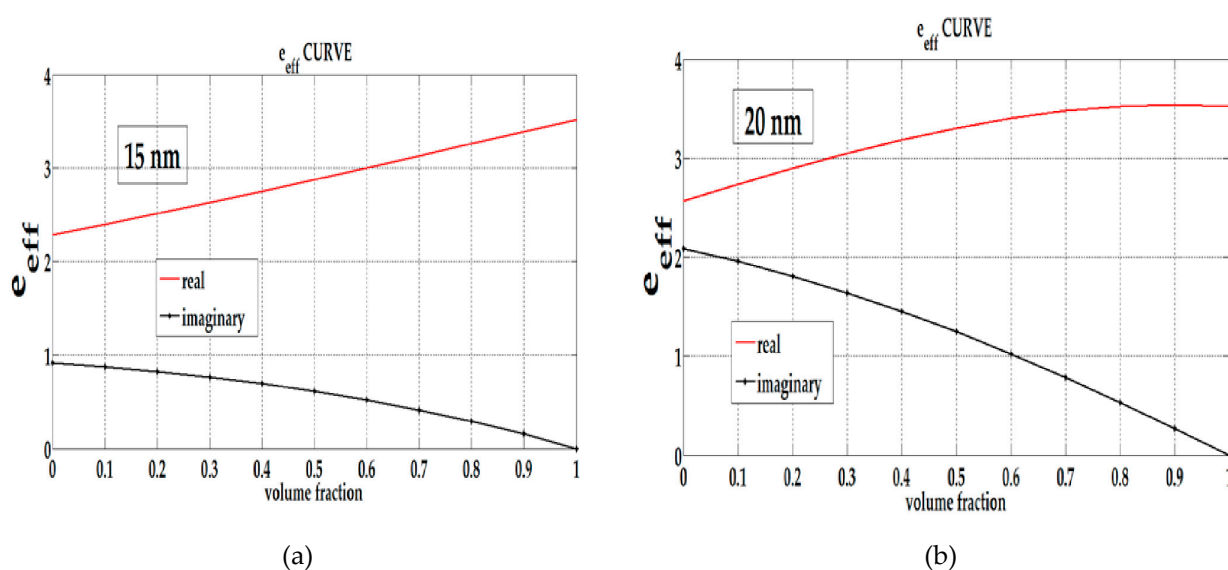
214   **Figure 9**. The composite effective permittivity with variation in the volume fraction (*F*) of
215   composite for fixed size of the core-shell (a) 15 nm(b) 20 nm.

216   The reflectivity from the SPR-based biosensor consisting of   nanoparticle core-shell is shown in
217   Figure 10 and Figure 11. If the layer only consists of a prism, a thin film of metal (40 nm Ag) and 20
218   nm biomolecule (conventional SPR), the dip of the ATR curve occurs at the incident angle 45.17°
219   (*solid line*). After the composite had been deposited onto the surface of the Ag thin film, the dip of the
220   reflectivity curve was shifted to the larger angle. Referring to Figure 10 for the volume fraction (*F*)=
221   0.1 and the Fe_3O_4@Au radius was varied from 5 nm to 20 nm, the SPR angle was shifted to the larger
222   angle. By increasing the radius of Fe_3O_4@Au, the angle of resonance increases as well. It can be seen
223   in Figure 10 that the minimum reflectivities are seen at 45.75° for thickness 5 nm and at 45.78° for 10
224   nm thickness, while from Figure 11, for the volume fraction(*F*)= 0.8 and the Fe_3O_4@Au radius was
225   varied from 5 nm to 20 nm, the SPR angle is shifted to the larger angle as well. The figure shows that
226   the minimum reflectivities occured at 47.38° for thickness 10 nm and at 47.55° for thickness 15 nm.
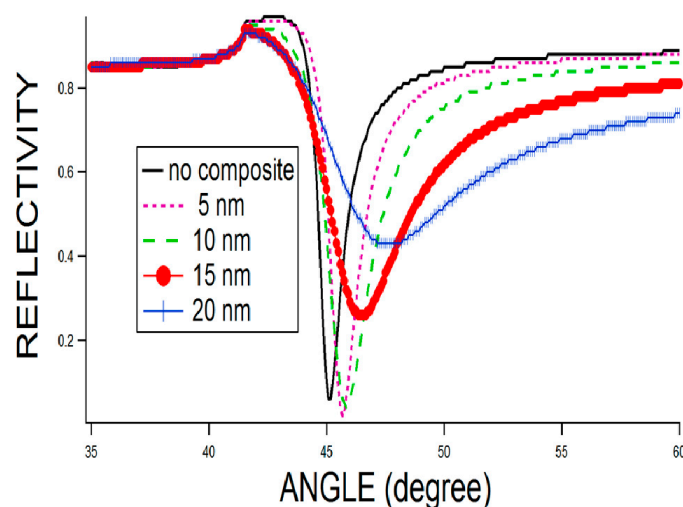
227   **Figure 10.** The ATR spectra for the volume fraction of the composite *F*=0.1. The radius of
228   inclusion material at *R*=20 nm and the radius of core-shell varied from 5 nm to the 20 nm
229   with fixed $(b/a)^3$=0.73.

Figure 11. The ATR spectra for the volume fraction of the composite F=0.8. The radius of inclusion material at R=20 nm and the radius of core-shell varied from 5 nm to the 20 nmwith fixed $(b/a)^3$=0.73.

Therefore, it can be obtained from Eq. 7 that for the core-shell radius 10 nm, the sensitivity increased by 1.35 % for F=0.1, and by 4.89 % for F =0.8 compared to the sensitivity of the conventional SPR-based biosensor without core-shell addition

5. Conclusions

In summary, we have presented a simulation for the size effect of the inclusion material in the SPR-based biosensor through the ATR spectra. Our calculations confirm that the property combination of the magnetic and plasmonic materials leads to the enhancement of the SPR-based biosensor sensitivity that applies to detect the existence of Hb as analyte. By varying the radii of the core (Fe_3O_4) and the shell (Au), the refractive index of the core-shell changes and leads to the change in the composite (core-shell+Hb+water) permittivity. The change in this effective permittivity results in the change of the dip position in the reflectivity spectrum to the larger angle. The SPR dips were shifted when the core-shell was added to the composite as the active material. This *large shift* in the *dip* angle suggests the potential for its application in the highly sensitive biosensor, in this case, sensing Hb as the analyte.

Author Contributions: Widayanti conceived the idea for the study, conceptualization, data curation, funding acquisition, methodology, software, visualization and writing original draft of the manuscript. Kamsul Abraha contributed to investigated, validated, writing-review & editing draft of the manuscript and Agung Bambang S.U contribute to helped for supervision and validation. Kamsul Abraha as the corresponding author for this manuscript. All author contributed significant effort to the manuscript preparation.

Conflicts of Interest: The authors declare no conflict of interest.

References

1. Wang, J.; Sun, Y.; Wang, L.; Zhu, X.; Zhang, H.; and Song, D. Surface plasmon resonance biosensor based on Fe3O4/Au nanocomposites. *Colloids and Surfaces B: Biointerfaces.* **2010**, 81, 600-606. https://doi.org/10.1016/j.colsurfb.2010.08.007.

257   2.   Agbor, N.E.; Cresswell, J.P.; Petty, M.C.; and Monkman, A.P. An optical gas sensor based on polyaniline
258   Langmuir-Blodgett films. *Sensors and Actuators B: Chemical*. **1997**, 41, 137-141.
259   https://doi.org/10.1016/S0925-4005(97)80286-9.

260   3.   Kretschmann, E.; Raether, H. Notizen: Radiative Decay of Non Radiative Surface Plasmons Excited by
261   Light.. *Zeitschrift Naturforsh.* **1968**, 23 A, 2135-2136, https://doi.org/10.1515/zna-1968-1247.

262   4.   Liedberg, B.; Nylander, C.; Lunström, I. Surface plasmon resonance for gas detection and biosensing.
263   *Sensors and Actuators.* **1983**, 4, 299-304. https://doi.org/10.1016/0250-6874(83)85036-7.

264   5.   He, L.; Musick, M.D.; Nicewarner, S.R; Salinas, F.G.; Benkovic, S.J.; Natan, M.J.; Keating, C.D. Colloidal
265   Au-Enhanced Surface Plasmon Resonance for Ultrasensitive Detection of DNA Hybridization. *Journal of*
266   *the American Chemical Society*. **2000,** 122, 9071-9077. https://pubs.acs.org/doi/abs/10.1021/ja001215b.

267   6.   Milkani, E.; Lambert, C.R.; Mc Gimpsey, W.G. Direct detection of acetylcholinesterase inhibitor binding
268   with an enzyme-based surface plasmon resonance sensor. *Anal Biochem*. **2011**, 408, 212-219.
269   https://doi.org/10.1016/j.ab.2010.09.009.

270   7.   Salamon, Z.; Macleod, H.A.; Tollin, G. Surface plasmon resonance spectroscopy as a tool for investigating
271   the biochemical and biophysical properties of membrane protein systems. II: Applications to biological
272   systems. *Biochimica et biophysica acta*. **1997**, 1331, 131-152. https://www.ncbi.nlm.nih.gov/pubmed/9325439..

273   8.   Sharma, A.K. Plasmonic biosensor for detection of hemoglobin concentration in human blood: Design
274   considerations. *Journal of Applied Physics*. **2013**, 114, 044701. https://doi.org/10.1063/1.4816272.

275   9.   Wu, L.; Chu, H.S.; Koh, W.S.; Li, E.P. Highly sensitive graphene biosensors based on surface plasmon
276   resonance. *Opt. Express*. **2010**, 18, 14395-14400. https://doi.org/10.1364/OE.18.014395.

277   10. Liang, R. P.; Yao, G. H.; Fan, L. X.; Qiu, J. D. Magnetic Fe3O4@Au composite-enhanced surface plasmon
278   resonance for ultrasensitive detection of magnetic nanoparticle-enriched α-fetoprotein. *Anal Chim Acta*.
279   **2012**, 737, 22-28https://doi.org/10.1016/j.aca.2012.05.043.

280   11. Frasconi, M.; Tortolini, C.; Botrè, F.; Mazzei, F. Multifunctional Au Nanoparticle Dendrimer-Based Surface
281   Plasmon Resonance Biosensor and Its Application for Improved Insulin Detection. *Analytical Chemistry*.
282   **2010**, 82, 7335-7342. https://doi.org/10.1021/ac101319k.

283   12. Baida, H.; Billaud, P.; Marhaba, S.; Christofilos, D.; Cottancin, E.; Crut, A.; Lermé, J.; Maioli, P.; Pellarin,
284   M.; Broyer, M.; Del Fatti, N.; Vallée, F.; Sánchez-Iglesias, A.; Pastoriza-Santos, I.; Liz-Marzán, L.M.
285   Quantitative Determination of the Size Dependence of Surface Plasmon Resonance Damping in Single
286   Ag@SiO2 Nanoparticles. *Nano Letters*. **2009**, 9, 3463-3469. https://doi.org/10.1021/nl901672b.

287   13. Zhu, J. Surface Plasmon Resonance from Bimetallic Interface in Au–Ag Core–Shell Structure Nanowires.
288   *Nanoscale Research Letters*. **2009**, 4, 977-981. https://dx.doi.org/10.1007%2Fs11671-009-9344-4.

289   14. Pathak, N.; Ji, A.; Sharma, R.P. Tunable Properties of Surface Plasmon Resonances: The Influence of
290   Core–Shell Thickness and Dielectric Environment. *Plasmonics*. **2014**, 9,651-657.
291   https://doi.org/10.1007/s11468-014-9677-4.

292   15. Ahmadi, N.; Poursalehi, R.; and Farshi, M.K.M. The Interparticle Coupling Effect on Plasmon Resonance
293   Properties of Magnetite@Au Magnetoplasmonic Nanoparticles. *Procedia Materials Science*. **2015**, 11,
294   254-258. https://doi.org/10.1016/j.mspro.2015.11.131.

295   16. Liu, Y.; Han, T.; Chen, C.; Bao, N.; Yu, C. M.; Gu, H. Y. A novel platform of hemoglobin on core–shell
296   structurally Fe 3O 4@Au nanoparticles and its direct electrochemistry. *Electrochimica Acta*. **2011**, *56*,
297   3238-3247, https://www.cheric.org/research/tech/periodicals/doi.php?art_seq=915551.

298   17.   Wang, J.; Song, D.; Zhang, H.; Zhang, J;, Jin, Y.; Zhang, H.; Zhou, H.; and Sun, Y. Studies of Fe3O4/Ag/Au
299   composites for immunoassay based on surface plasmon resonance biosensor. *Colloids and surfaces. B,*
300   *Biointerfaces.* **2013**, 102, 165-170. https://doi.org/10.1016/j.colsurfb.2012.08.040.

301   18.   Zhou, H.; Lee, J.; Park, T.J.; Lee, S.; and Park, J. Ultrasensitive DNA monitoring by Au-Fe3O4
302   nanocomplex. *Sensors and Actuator B: Chemical.* **2012**, 163, 224-232,
303   http://dx.doi.org/10.1016%2Fj.snb.2012.01.040.

304   19.   Chen, H.; Qi, F.; Zhou, H.; Jia, S.; Gao, Y.; Koh, K.; and Yin, Y. Fe3O4@Au nanoparticles as a means of
305   signal enhancement in surface plasmon resonance spectroscopy for thrombin detection. *Sensor and*
306   *Actuator B: chemical.* **2015**, *212*, 505-511, https://doi.org/10.1016/j.snb.2015.02.062.

307   20.   Guo, X. Fe3O4@Au nanoparticles enhanced surface plasmon resonance for ultrasensitive immunoassay.
308   *Sensor and Actuator.* **2014**, *205*, 276-280, http://dx.doi.org/10.1016%2Fj.snb.2014.08.055.

309   21.   Sharma, A.K.; Jha, R.; Pattanaik, H. S. Design considerations for surface plasmon resonance based
310   detection of human blood group in near infrared.   *Journal of Applied Physics*, **2010**, 107, 034701.
311   https://doi.org/10.1063/1.3298503.

312   22.   Stuart, D.A.; Haes, A.J.; Yonzon, C.R.; Hicks, E.M.; Van Duyne, R.P. Biological applications of localized
313   surface plasmonic phenomenae.   *IEE proceedings. Nanobiotechnology*. **2005**, 152, 13-32. doi:
314   10.1049/ip-nbt:20045012.

315   23.   Jain, P.K.; Huang, X.; El Sayed, I.H.; El-Sayed, M.A. Review of some interesting surface plasmon
316   resonance-enhanced properties of noble metal nanoparticles and their applications to biosystems'.
317   *Plasmonics*. **2007**, 2, 107-118. https://doi.org/10.1007/s11468-007-9031-1.

318   24.   Zhernovaya, O.; Sydoruk, O.; Tuchin, V.; Douplik, A. The refractive index of human hemoglobin in the
319   visible range.   *Physics in Medicine and Biology*.   **2011**, 56, 4013-4021.
320   https://doi.org/10.1088/0031-9155/56/13/017.

321   25.   Johnson, P.B.; and Christy, R.W. Optical Constants of the Noble Metals. *Physical Review B*. **1972**, 6,.
322   4370-4379. https://doi.org/10.1103/PhysRevB.6.4370.

323   26.   Rather, H. *Surface Plasmons on Smooth and Rough Surfaces and Gratings*,; Springer-Verlag, Berlin. **1986**, ISBN
324   978-3-540-47441-8.   https://books.google.co.id/books?id=3rsdAQAAMAAJ.

325   27.   Schlegel, A.; Alvarado, S.F.; and Wachter, P. Optical properties of magnetite (Fe$_3$O$_4$). *Journal of Physics C:*
326   *Solid State Physics*. **1979**, 12, 1157-1164. https://doi.org/10.1088/0022-3719/12/6/027.

327   28.   Chettiar, U.K.; Engheta, N. Internal homogenization: Effective permittivity of a coated sphere. *Opt.*
328   *Express*.   **2012**, 20, 22976-22986. https://doi.org/10.1364/OE.20.022976.

329   29.   XUE, Q. Effective-medium theory for two-phase random composites with an interfacial shell. *J. Mater.*
330   *Sci. Technol*. **2000**, 16, 367-369. http://www.jmst.org/CN/Y2000/V16/I04/367.

331   30.   Verma, R.; Gupta, B.D.; Jha, R. Sensitivity enhancement of a surface plasmon resonance based
332   biomolecules sensor using graphene and silicon layers. Sensors & Actuators: B. Chemical. **2011**, 160,
333   623-631. https://doi.org/10.1016/j.snb.2011.08.039.